Title	Photon assisted tunneling through three quantum dots with spin-orbit-coupling
Author(s)	Tang, HZ; An, X; Wang, AK; Liu, JJ
Citation	Journal of Applied Physics, 2014, v. 116, article no. 063708
Issued Date	2014
URL	http://hdl.handle.net/10722/206813
Rights	Creative Commons: Attribution 3.0 Hong Kong License

Photon assisted tunneling through three quantum dots with spin-orbit-coupling

Han-Zhao Tang,[1] Xing-Tao An,[2,3,a)] Ai-Kun Wang,[2] and Jian-Jun Liu[1,4,b)]
[1]*College of Physical Science and Information Engineering and Hebei Advanced Thin Film Laboratory, Hebei Normal University, Shijiazhuang 050024, China*
[2]*School of Sciences, Hebei University of Science and Technology, Shijiazhuang, Hebei 050018, People's Republic of China*
[3]*Department of Physics and Center of Theoretical and Computational Physics, University of Hong Kong, Hong Kong*
[4]*Physics Department, Shijiazhuang University, Shijiazhuang, Hebei 050035, China*

(Received 5 March 2014; accepted 30 July 2014; published online 12 August 2014)

The effect of an ac electric field on quantum transport properties in a system of three quantum dots, two of which are connected in parallel, while the third is coupled to one of the other two, is investigated theoretically. Based on the Keldysh nonequilibrium Green's function method, the spin-dependent current, occupation number, and spin accumulation can be obtained in our model. An external magnetic flux, Rashba spin-orbit-coupling (SOC), and intradot Coulomb interactions are considered. The magnitude of the spin-dependent average current and the positions of the photon assisted tunneling (PAT) peaks can be accurately controlled and manipulated by simply varying the strength of the coupling and the frequency of the ac field. A particularly interesting result is the observation of a new kind of PAT peak and a multiple-PAT effect that can be generated and controlled by the coupling between the quantum dots. In addition, the spin occupation number and spin accumulation can be well controlled by the Rashba SOC and the magnetic flux. © *2014 AIP Publishing LLC*. [http://dx.doi.org/10.1063/1.4892822]

I. INTRODUCTION

Electron transport through low dimensional nanostructures to which a microwave (MW) field is applied has received increased attention in recent years. An important characteristic of these systems is that the electron in the system can exchange an energy $n\hbar\omega$ with the external fields, where $n = \pm 1, \pm 2, \ldots$, and ω is the frequency of the external field, thus leading to several new inelastic tunneling channels. This phenomenon has been called the photon assisted tunneling (PAT) effect.

The effects of a MW field on superconductivity were investigated by Tien *et al.*[1] in the 1960s. Later, different theoretical methods were proposed, such as the time-dependent Schrödinger equation,[2–4] the transfer Hamiltonian method,[5,6] the Master equation,[7,8] and the Keldysh nonequilibrium Green's function method.[9–14] Experimentally, the PAT effect has been observed in quantum dot (QD) systems with a single QD[15] and in a system with double QDs.[16–18] The observation of the photon-electron pump phenomenon in a QD system which is controlled by an ac field has been reported by Kouwenhoven *et al.*[19,20] Sun *et al.* have investigated electron tunneling through a QD[21] and a quantum-dot-molecule[22] irradiated by a MW field. Besides the single QD system, time-dependent tunneling through double[23–25] and triple[26,27] coupled QDs has also received great attention both experimentally and theoretically in many cases because of the potential applications in quantum computing devices.

When a device is prepared in a semiconductor with a perpendicular electric field, Rashba spin-orbit-coupling (SOC) will appear in the system, which leads to a nonzero spin-dependent phase σ_R.[28] In addition, the time reversal symmetry can be broken by a magnetic flux φ. If both these effects are present, the average current is expected to become spin polarized. Lü *et al.*[26] have proposed a spin filter using a triple QD system with dc bias. However, to the best of our knowledge, little attention has been paid to spin-dependent transport in such device in a MW field, especially a system with Rashba SOC. In order to study the impact of coupling between QDs in a device with three QDs, we have constructed a theoretical model to investigate the PAT effect and electron-photon pump phenomenon when the Coulomb interaction, Rashba SOC, and an external magnetic field are all considered.

In this paper, using the Keldysh nonequilibrium Green's function method, we calculate the time-dependent current through two QDs connected in parallel with a side-coupled QD, the whole system being irradiated by a MW field. This paper is organized as follows. The model and analytic method are introduced in Sec. II. In Sec. III, we discuss our results, including the spin-dependent average current, the occupation number, and the spin accumulation for various cases. Finally, a summary is given in Sec. IV.

II. THEORETICAL MODEL

As shown in Fig. 1, the system we propose is composed of three QDs, which can also be seen as two QDs connected in parallel with a third side-coupled QD. The third QD is not

a)Electronic mail: anxt@hku.hk
b)Electronic mail: liujj@mail.hebtu.edu.cn

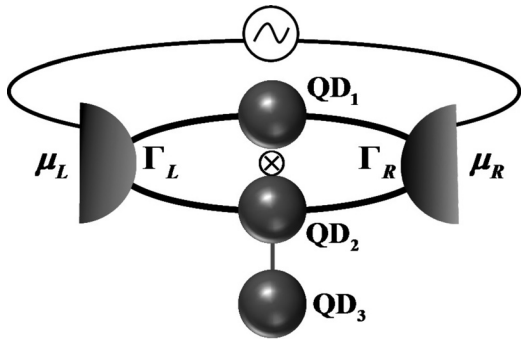

FIG. 1. Schematic diagram of a device consisting of two QDs connected in parallel with a third side-coupled QD connected to one of the other QDs. An ac bias is applied across the leads.

directly coupled to the leads under ac bias. The Hamiltonian of the system can be described as follows:

$$H = \sum_{\beta=L,R} H_\beta + H_D + H_T. \tag{1}$$

The first term of the Hamiltonian in Eq. (1) describes the lead system

$$H_\beta = \sum_{k,s} \varepsilon_{\beta k}(t)\alpha^\dagger_{\beta ks}\alpha_{\beta ks}, \tag{2}$$

where $\alpha^\dagger_{\beta ks}(\alpha_{\beta ks})$ is the creation (annihilation) operator of an electron with spin s ($s=\uparrow,\downarrow$) and Bloch wave vector k in the β lead. The β lead is the left lead or the right lead in the system. The electron energy $\varepsilon_{\beta k}(t) = \varepsilon^0_{\beta k} + eV + W_\beta(t) = \varepsilon^0_{\beta k} + eV_\beta - eW_\beta\cos(\omega t)$. Here, $\varepsilon^0_{\beta k}$ is a single particle energy, V_β is a dc bias (electron charge $-e$), and the ac bias of frequency ω is given by $W_\beta\cos(\omega t)$. The effect of ac fields influencing the energy levels of the source and the drain has been studied by Jauho *et al.*[11]

The second term in Eq. (1) describes the QD system

$$H_D = \sum_{s,i=1,2,3} \varepsilon_i(t)d^\dagger_{is}d_{is} - (td^\dagger_{2s}d_{3s} + H.c.) + U_i d^\dagger_{i\uparrow}d_{i\uparrow}d^\dagger_{i\downarrow}d_{i\downarrow}, \tag{3}$$

where $d^\dagger_{is}$ (d_{is}) creates (annihilates) an electron in the ith QD with energy level $\varepsilon_i(t) = \varepsilon^0_i - eW_D\cos(\omega t)$; ε^0_i is the single particle energy in the ith QD. t is the coupling between the QD_2 and the QD_3 and U_i describes the Coulomb repulsion energy of the ith QD. To simplify the calculation, we assumed that $U_i = U$ in this paper.

The last term in Eq. (1), H_T, describes electron tunneling between the QDs and leads

$$H_T = \sum_{k,s,\beta,i=1,2} t_{\beta is}\alpha^\dagger_{\beta ks}d_{is} + H.c., \tag{4}$$

where $t_{\beta is}$ represents the QDs-lead coupling.

According to Ref. 28, the Rashba SOC has two main effects in a QD system: (1) an extra spin-dependent phase factor appears in the tunneling matrix and (2) interlevel spin-flip can be induced by Rashba SOC, but not intralevel spin-flip. To simplify the calculation, we assume that each QD has a single energy level. Thus only the first of these two effects is taken into account in the present work. In order to simplify the analysis of the self-energies, we use the wide-band limit (WBL), which is an approximation. The energy dependence of the coupling between the leads and the QDs can be neglected by using the WBL. In the WBL, we can use the bandwidth functions to express the retarded self-energy

$$\Sigma^r_{\beta s}(t,t') = -\frac{i}{2}\delta(t-t')\Gamma^\beta_s, \tag{5}$$

where $\Gamma^\beta_{sij}(\varepsilon,t,t') = 2\pi\rho_\beta t_{\beta,i}t^*_{\beta,j}\exp\{i\int_{t'}^{t} W_\beta(\tau)d\tau\}$. Here, ρ_β describes the spin density of states in the β lead for spin channel s. Therefore, we can use the general time-dependent current method proposed by Wingreen *et al.*[10] and obtain the time-dependent current $I(t)$ ($\hbar = 1$)

$$I_{\beta s}(t) = -2e\mathrm{Im}\int_{-\infty}^{t} dt' \int \frac{d\varepsilon}{2\pi} Tr\Big\{e^{-i\varepsilon(t'-t)} \times \Gamma^\beta_s(\varepsilon,t,t') \times \left[G^<_s(t,t') + f_\beta(\varepsilon)G^r_s(t,t')\right]\Big\}, \tag{6}$$

in which $f_\beta(\varepsilon)$ is the Fermi distribution function of electrons in the β lead. Both the retarded and lesser Green's functions are required. Using the Dyson equation, the retarded Green's function G^r of the system can be obtained from the free Green's function of the QDs without couplings to the leads

$$G^r_s(t,t') = \int \frac{d\varepsilon}{2\pi}\exp\left[-i\varepsilon(t-t') - i\int_{t'}^{t} d\tau W_D\cos(\omega\tau)\right]G^r_s(\varepsilon), \tag{7}$$

$$G^r_s(\varepsilon) = [g^{r-1}_s(\varepsilon) - \Sigma^r_s(\varepsilon)]^{-1}, \tag{8}$$

where $g^r_s(\varepsilon)$ can be obtained from the Fourier transformation of $g^r_{ii}(t,t') = -i\theta(t-t')e^{-i\int_{t'}^{t}\varepsilon_i(t_1)dt_1}$. The quantity n_{is} is the average occupation number and can be calculated using the self-consistent values of n_{is}: $n_{is} = \mathrm{Im}\langle G^<_{iis}(t,t)\rangle$. As for the lesser Green's function $G^<$, we use the Keldysh relation, $G^< = G^r\Sigma^<G^a$, which can be easily calculated when G^r is known. Using Eqs. (7) and (8), Eq. (6) is reduced to the form

$$I_{\beta s}(t) = -e\int\frac{d\varepsilon}{2\pi}\mathrm{Im}\Big\{2f_\beta(\varepsilon)\Gamma^\beta_s A_{\beta s}(\varepsilon,t) + i\Gamma^\beta_s\sum_{\alpha=L,R} f_\alpha(\varepsilon)A_{\alpha s}(\varepsilon,t)\Gamma^\alpha_s A^\dagger_{\alpha s}(\varepsilon,t)\Big\}, \tag{9}$$

where

$$A_{\beta s}(\varepsilon,t) = \exp\left[i(eW_\beta - eW_D)\sin(\omega t)/\omega\right] \times \sum_n J_n\left(e\frac{W_D - W_\beta}{\omega}\right)e^{in\omega t}G^r_s(\varepsilon_n). \tag{10}$$

Here, J_n is Bessel function and $\varepsilon_n = \varepsilon - n\omega$. Equation (9) is the expression for the instantaneous current. However, experimentally the average current is more relevant. The time average of Eq. (9) is

$$\langle I\rangle = 2e\int\frac{d\varepsilon}{2\pi}\sum_n Tr\Big\{\Big[J^2_n\left(e\frac{W_D - W_L}{\omega}\right)f_L(\varepsilon) - J^2_n\left(e\frac{W_D - W_R}{\omega}\right)f_R(\varepsilon)\Big]\Gamma^L_s G^r_s(\varepsilon_n)\Gamma^R_s G^a_s(\varepsilon_n)\Big\}. \tag{11}$$

III. RESULTS AND DISCUSSION

A. Parallel double dots ($t = 0$)

While the transport properties of single and double QDs have been well studied,[15] for completeness and for later discussions, we analyse parallel double QDs without a side-coupled third QD in this subsection. We used ω as the units of measurement and assumed that $\Gamma_1^\beta = \Gamma_2^\beta = \Gamma = 0.3$. Using the Eq. (11), the spin-dependent average current of the model can be numerically simulated. In our calculation, we found that the case in which external ac fields are applied symmetrically ($W_L = W_R$) on the leads is same as the case in which the external MW fields are applied directly to the QDs.[21] Therefore, we take $W_D = 0$ in our discussion. We begin discussion of the double QDs with both the Rashba SOC and the magnetic field considered in a symmetric ac field. For this situation, Fig. 2 shows the spin-dependent average currents as a function of the energy level of the QDs.

As illustrated in Fig. 2(a), the dc current (black solid line) has a Lorentzian line shape whose width is determined by Γ. The peak of the average current occurs at $\varepsilon = 0$. There is no spin splitting when the system does not have either Rashba SOC or a magnetic field. In addition, when a harmonic ac source with amplitude $eW_{L,R}/\hbar\omega = 1$ (blue solid line) is applied, changes caused by the ac field can be discerned. The current shows two polar values at $\varepsilon = \pm\hbar\omega$. The photo-assisted features are more clearly seen when $eW_{L,R}/\hbar\omega = 2$ (red solid line), in which there are side peaks located at $\varepsilon = \pm\hbar\omega$ and $\varepsilon = \pm 2\hbar\omega$. These peaks are due to the PAT or sideband effect, and each term in the summation of Eq. (11) can be regarded as the contribution of the n-photon process

$$\varepsilon = n\hbar\omega, \quad n = 0, \pm 1, \pm 2, \ldots. \tag{12}$$

The average current, shown in Fig. 2(a), is symmetric about $\varepsilon = 0$ when the dc source-drain voltage $V = \mu_L - \mu_R = 0.1$. From the PAT point of view, the part of average current with $\varepsilon < 0$ is associated with first absorption and then emission of photons, while the part for $\varepsilon > 0$ is associated with first emission and then absorption, i.e., the time reversed counterpart to $\varepsilon < 0$. In addition, the central peak at $\varepsilon = 0$ is suppressed which is due to the prefactor $J_n^2(e\frac{W_D - W_L}{\omega})f_L(\varepsilon) - J_n^2(e\frac{W_D - W_R}{\omega})f_R(\varepsilon)$ in each term of the summation in Eq. (11), which causes the peak heights for resonant tunneling to become lower for larger n. It can be obtained in our calculation that the sum of the heights of all peaks is equal to the height of the original peak.

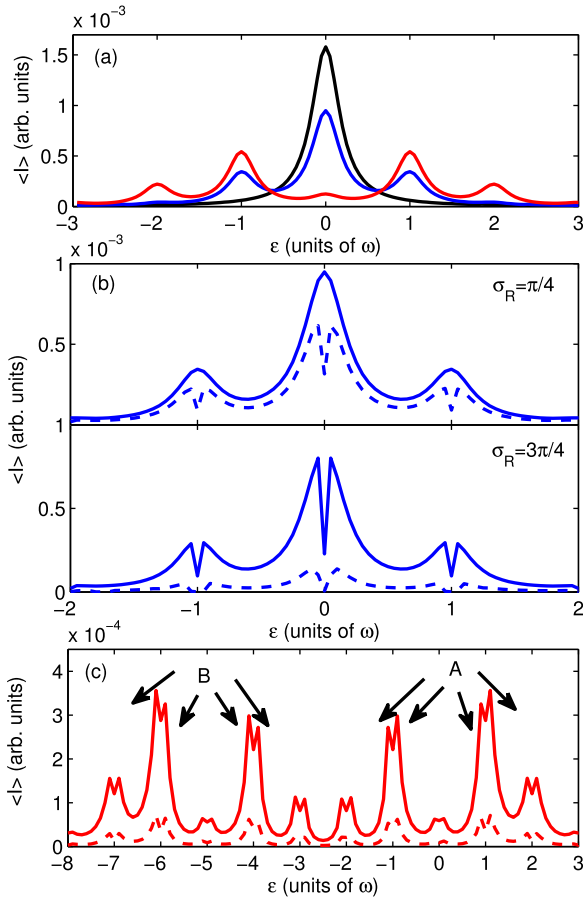

FIG. 2. Spin-dependent average currents, $\langle I\rangle_\uparrow$ (solid line) and $\langle I\rangle_\downarrow$ (dashed line), for QDs in parallel as a function of the electron energy level ε in the QDs under ac bias with $eW_{L,R} = 0$ (black line), $eW_{L,R} = 1$ (blue line), and $eW_{L,R} = 2$ (red line) (a) without Rashba SOC, magnetic field, and Coulomb interaction; (b) with magnetic flux $\varphi = \pi/4$ and no Coulomb interaction; and (c) with Rashba SOC ($\sigma_R = 3\pi/4$), magnetic flux ($\varphi = \pi/4$), and Coulomb interaction ($U = 5$). The other parameters are $\hbar\omega = 1$, $k_BT = 0.001$, and $V = 0.1$.

In the Fig. 2(b), we show the spin-dependent average current when the Rashba SOC and magnetic field are both included. The results show that the spin-dependent average current $\langle I\rangle$ of the two spin channels is equal in the absence of both Rashba SOC and a magnetic field, but becomes quite different when they are included. There are two remarkable features in the average current characteristics that arise due to Rashba SOC and the magnetic field. Firstly, as shown in Fig. 2(b), when the magnetic field phase is $\varphi = \pi/4$ and the Rashba SOC phase is $\sigma_R = \pi/4$, all peaks of the spin down current, including the main peaks and sideband peaks, are split at $\varepsilon = n\hbar\omega$. However this splitting phenomenon does not occur in the spin up current when $\sigma_R = \pi/4$, see Fig. 2(b). The reason is that the sum of the phases is $-s\sigma_R + \varphi = 0$ for the spin up current ($s = 1$), but the sum is $-s\sigma_R + \varphi = \pi/2$ for the spin down current ($s = -1$). The Rashba SOC behaves like a momentum dependent magnetic field which is perpendicular to the system. This effective magnetic field induces a spin-dependent phase difference between the electrons traveling clockwise and counterclockwise between QD_1 and the QD_2. Because of the interference between the wave functions along the two paths when $\sigma_R = \pi/4$, the current shows a large decrease at $\varepsilon = n\hbar\omega$ for the spin down channel. As a result, the spin down channel peaks are split at $\varepsilon = n\hbar\omega$.

Secondly, the Rashba SOC is the result of the torque of the external electrical field on a moving spin in the system,[28] which can induce a spin-dependent phase difference for spin up and spin down electrons transmitted in the QDs. By adjusting the strength of the Rashba SOC, we can control the spin up current, spin down current, and the polarization. In Fig. 2(b), when $\sigma_R = 3\pi/4$, we can note the zero current at $\varepsilon = 0$ and $\varepsilon = \pm\hbar\omega$ in the spin down channel. However,

non-zero currents occur at the same values of ε for the spin up channel. Therefore, a 100% spin up current can be obtained at $\varepsilon = 0$ and $\varepsilon = \pm\hbar\omega$. Based on our calculation, the curves of current for the spin up and spin down channels are interchanged when $\sigma_R = -3\pi/4$ (not shown in figure). Therefore, the direction of spin polarization can be controlled by the Rashba SOC σ_R, which is useful for designing a spin filter under ac bias.

We can also note that there are two kinds of peak in Fig. 2(c) which is distinguished by having a non-zero Coulomb interaction. The A-type peaks are the general PAT peaks discussed above for both spin directions and are a distance $\varepsilon = \pm n\hbar\omega$ away from the main peak at $\varepsilon = 0$. The "B" peaks are also a kind of PAT peaks but their positions are modified due to the Coulomb interaction. The first "B" peak is located at $\varepsilon = -U + 2\hbar\omega$. The electronic states in the QDs are occupied with energy $\varepsilon = -U$, and peaks at $\varepsilon = -U \pm n\hbar\omega$ produce as the result of a PAT process based on a QD with this energy. In this case, due to the Coulomb interaction, a photon must have an energy $\varepsilon = -U \pm n\hbar\omega$ in order for it to be absorbed or emitted.

Fig. 3(a) shows that the average current $\langle I \rangle$ versus the intradot energy ε when the system is subject to an asymmetrical time-dependent external field ($W_L = 0$ and $W_R \neq 0$) for $\sigma_R = 0$, $\pi/4$, $\pi/2$, and $3\pi/4$. When $\sigma_R = 0$, the main peak is located at $\varepsilon = \Gamma^{L(R)}$. For $\sigma_R \neq 0$, the subsidiary peak exceeds the main peak (near $\varepsilon = \pm\hbar\omega$) and cannot be neglected. The shoulder on the left side of the main resonant peak and a negative current on the right side in Fig. 3(a) result from the electron-photon pump. With increasing σ_R, the magnitude of the average current is reduced and the shoulder becomes clearer, but the location of the PAT peaks is independent of the strength of the Rashba SOC. The distance between the PAT peaks and the point $\varepsilon = 0$ is almost unchanged and is equal to $\varepsilon = \pm\hbar\omega$.

It should be noted that when both φ and σ_R are taken into account, the current is spin polarized and can be controlled. In Fig. 3(b), when the system is subject to an asymmetric time-dependent field, if $-0.8 < \varepsilon < 0$, the spin up current $\langle I \rangle_\uparrow$ is positive, which means that the spin up current $\langle I \rangle_\uparrow$ flows along the positive direction (left to right), while the spin down current $\langle I \rangle_\downarrow$ flows in the negative direction (right to left). In the range $0 < \varepsilon < 0.8$, however, the opposite situation occurs. This means that the current is spin polarized and the polarization can be controlled by the magnetic field and Rashba SOC in the asymmetric MW situation. Here, we should point out that since the intradot Coulomb interaction is considered in our model, we obtain a series of Coulomb oscillation shoulders in Fig. 3(c) located at $\varepsilon = -U \pm \hbar\omega$. To make clear the Coulomb oscillation shoulders, we set $\Gamma = 0.1$ in Fig. 3(c).

If we use ω as the measurement, we can obtain the current versus ω when the system is subject to an asymmetrical ac field ($W_L = 0$ and $W_R \neq 0$). The current curve should contain resonant peaks at $\hbar\omega = \varepsilon - U$ and $\hbar\omega = \varepsilon$. The frequency difference of the two resonant peaks is the magnitude of the Coulomb energy U. For a typical QD of 200 nm size (Coulomb energy $U \approx 1.8$ meV (Ref. 29)), the current curve should contain a PAT peak due to electrons

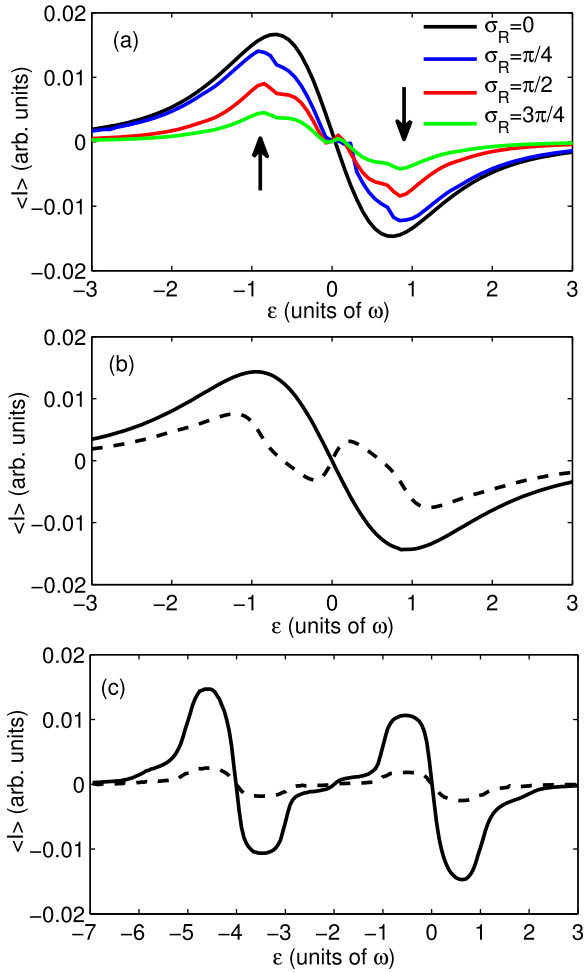

FIG. 3. For the asymmetric case ($eW_L = 0$, $eW_R = 1$), the spin-dependent average currents, $\langle I \rangle_\uparrow$ (solid line) and $\langle I \rangle_\downarrow$ (dashed line), are shown as a function of the electron energy level ε of the QDs under an asymmetric ac bias (a) with different strengths of Rashba SOC, $\varphi = 0$, and $U = 0$; (b) with $\varphi = \pi/4$, $\sigma_R = \pi/4$, and $U = 0$; (c) with $\varphi = \pi/4$, $\sigma_R = \pi/4$, and $U = 4$. The other parameters are $\hbar\omega = 1$, $k_B T = 0.001$, and $V = 0$. The arrows in (a) indicate the location of the shoulders.

with energy $\varepsilon - U$ absorbing a photon energy $\hbar\omega$ and then transmitting through the QDs, and a resonant peak due to electrons with energy ε tunneling through the QDs. The distance between the PAT peak and the resonant peak should be approximately 1.8 meV.

Spin polarization of the average current cannot realized by Rashba SOC alone; see Fig. 3(a). However the occupation number can be polarized by the SOC alone. To make clear the effect of Rashba SOC in our model, we introduce the total effective coupling strength T_{L1} between the QDs (e.g., QD_1) and the left lead

$$T_{L1s} = |t_{L1s} + t_{L2s} g^r_{22} t_{R2s} (-i\pi\rho) t_{R1s} e^{-is\sigma_R}|^2, \quad (13)$$

$$T_{R1s} = |t_{R1s} e^{-is\sigma_R} + t_{R2s} g^r_{22} t_{L2s} (-i\pi\rho) t_{L1s}|^2. \quad (14)$$

Due to the fact that $\sigma_R \neq 0$, we can see $T_{Lis} \neq T_{Ris}$ which causes spin accumulation ($\Delta n_i = \Delta n_{i\uparrow} - \Delta n_{i\downarrow}$) in the QDs. The spin up and spin down occupation numbers and the spin accumulation versus the intradot energy level ε in the QDs are shown in Figs. 4(a) and 4(b), respectively, for $\sigma_R = \pi/4$

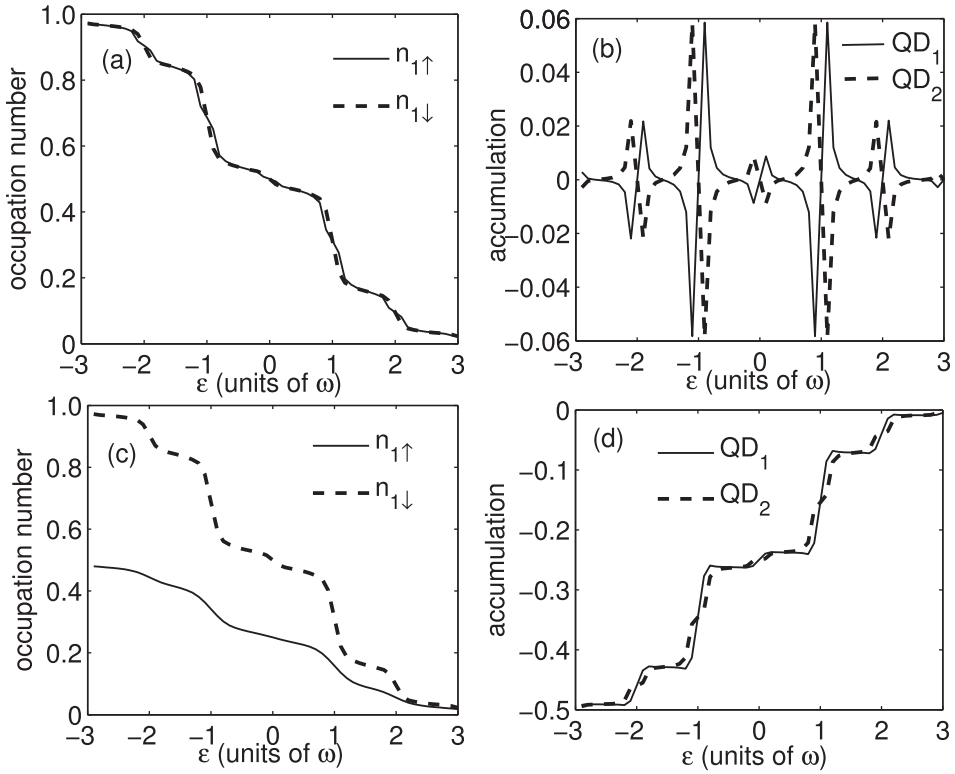

FIG. 4. (a) Spin occupation numbers $n_{1\uparrow}$, $n_{1\downarrow}$ and (b) accumulations Δn_1, Δn_2 versus electron energy ε in QDs when $\sigma_R = \pi/4$ and $\varphi = 0$. (c) Spin occupation numbers $n_{1\uparrow}$, $n_{1\downarrow}$ and (d) accumulations Δn_1, Δn_2 versus electron energy ε in QD_1 when $\sigma_R = \pi/4$ and $\varphi = \pi/4$. The other parameters are $eW_{L,R} = \hbar\omega = 1$, $k_BT = 0.001$, $V = 0.2$, and $U = 0$.

when the system is under a symmetric time-dependent external field ($eW_{L,R} = \hbar\omega = 1$). The spin occupation number $n_{i\uparrow}$ is not equal to $n_{i\downarrow}$ when the Rashba SOC is considered. As a result, the intradot spin accumulation Δn_i is non-zero. The spin accumulation in QD_1 is opposite to that in QD_2, see Fig. 4(b). At $\varepsilon = n\hbar\omega$, the spin accumulation $\Delta n_1 = \Delta n_2 = 0$. In the vicinity of the $\varepsilon = n\hbar\omega$, however, the spin accumulation Δn_i has a maximum value, which leads to a large polarization of one QD. However the spin accumulation of the system as a whole is zero for any ε, with the result that a net spin polarization does not form in double QD systems. Even for a small σ_R and dc bias V, the two QDs have polarizations with opposite signs. This enables us to control the spin accumulation using Rashba SOC. It would appear that the production of spin occupation and accumulation should be experimentally feasible with present nanotechnology.

The spin precession angle can be described as $\sigma_R = \alpha_R m^* L/\hbar^2$, and the strength of the Rashba SOC is about 3×10^{-11}eVm, which can be controlled experimentally. Here, L is the size of the QD. The magnitude of σ_R can reach yet larger values experimentally when the dimension of the QD is about 100 nm and $m^* = 0.036m_e$.[30] Figs. 4(c) and 4(d) describe the dependence of the intradot spin occupation numbers and the spin accumulation on the energy level ε in the QDs for the case $\sigma_R = \pi/4$ and $\varphi = \pi/4$. Spin accumulation in the QDs presents a "step" shape when φ and σ_R are both considered, see the Fig. 4(d). This is quite different from the situation in Fig. 4(b) where only σ_R is considered. It may be seen that the width of the "steps" is just $\hbar\omega$. Even for a small φ, Δn is large. For example, at $\varepsilon = -3\hbar\omega$, $\Delta n_i \approx -0.5$; which is quite large for a spin polarization that relies on small values of φ and σ_R without Coulomb interaction.

We now investigate the effect of the interaction between the electrons in the QDs system. The spin-dependent average currents versus the dc bias V for different strengths of the Coulomb interaction are shown in Fig. 5. From Fig. 5, we can see that spin polarization of the average current indeed occurs in the QDs with a finite dc bias V in the ac field. When the bias $V = 0$, the average current for both the spin up and spin down channels should be zero. The magnitude of the spin polarization increases when the dc bias V increases, and the spin polarized direction can be reversed by reversing the dc bias. Thus the direction and the magnitude of the spin

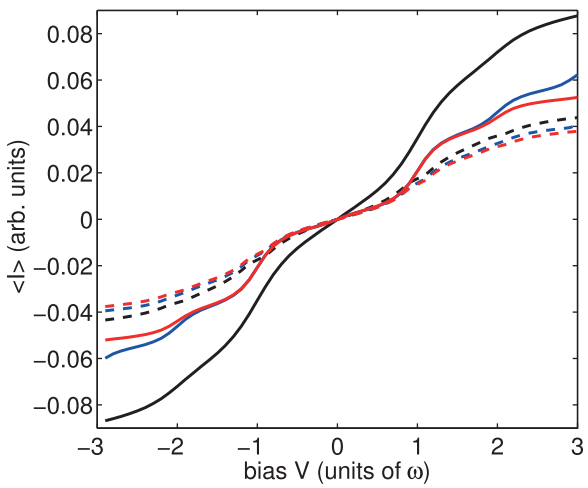

FIG. 5. Spin-dependent average current, $\langle I\rangle_\uparrow$ (solid line) and $\langle I\rangle_\downarrow$ (dashed line), versus dc bias V with a symmetric ac bias ($eW_{L,R} = \hbar\omega = 1$) and $U = 0$ (black curve), $U = 2$ (blue curve), and $U = 6$ (red curve). The other parameters are $k_BT = 0.001$, $\varepsilon = 0$, $\sigma_R = \pi/4$, and $\varphi = \pi/4$.

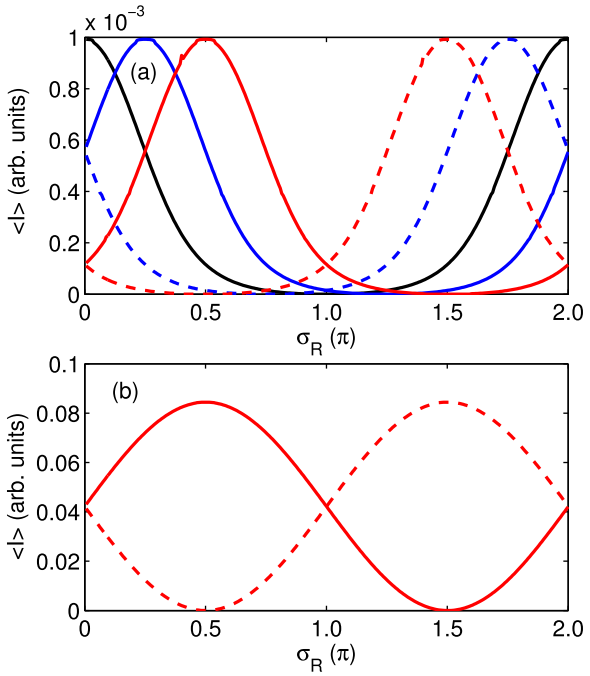

FIG. 6. Spin-dependent average current, $\langle I\rangle_{\uparrow}$ (solid line) and $\langle I\rangle_{\downarrow}$ (dashed line), versus the strength of Rashba SOC σ_R under a symmetric ac bias ($eW_{L,R} = \hbar\omega = 1$) with (a) $\varphi = 0$ (black curve), $\varphi = \pi/4$ (blue curve), $\varphi = \pi/2$ (red curve) and $V = 0.1$ (b) $\varphi = \pi/2$ and $V = 3$. The other parameters are $k_BT = 0.001$, $\varepsilon = 0$, and $U = 0$.

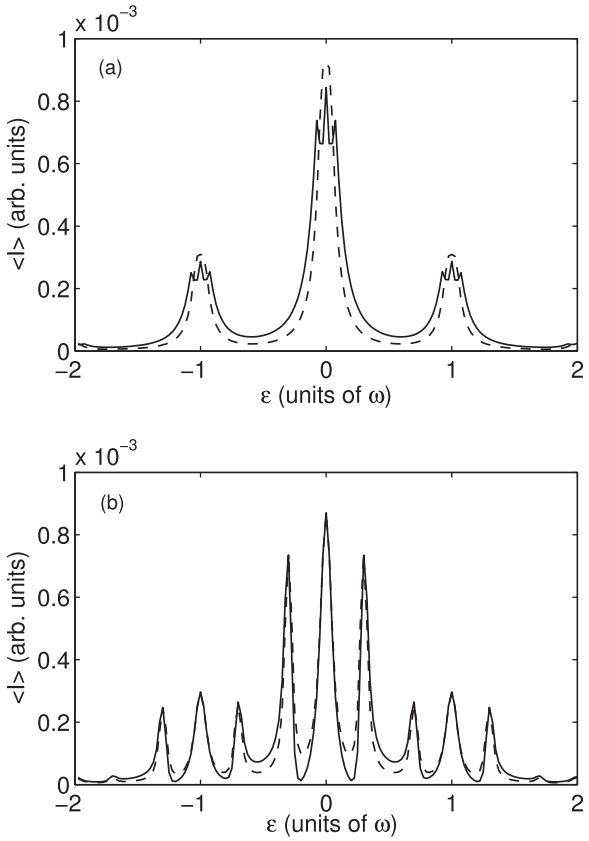

FIG. 7. Spin-dependent average current, $\langle I\rangle_{\uparrow}$ (solid line) and $\langle I\rangle_{\downarrow}$ (dashed line), versus electron energy ε under symmetric ac bias ($eW_{L,R} = \hbar\omega = 1$) with (a) $t = \Gamma = 0.1$ and (b) $t = 3\Gamma = 0.3$. The other parameters are $k_BT = 0.001$, $V = 0.1$, $\sigma_R = 3\pi/4$, $\varphi = \pi/4$, and $U = 0$.

polarization are easily regulated by the dc bias in a symmetric ac field. Fig. 5 also illustrates that the change in the spin down current in our model is tiny for any value of U and any dc bias voltage, whereas the spin up current has a finite value and decreases as U increases. Repulsion between electrons with spin up or spin down results from the Coulomb interaction, U, which leads to a reduction in the magnitude of spin polarization. The shoulders that appear at $V = \pm 1$ and $V = \pm 2$ are attributed to the PAT effect in the symmetric ac field.

Next, we study how the spin-dependent currents change with the strength of the Rashba SOC, σ_R. The average currents $\langle I\rangle$ versus the σ_R are illustrated in Fig. 6 from which we can see that the value of $\langle I\rangle$ is sensitive to the spin-dependent phase σ_R. The period of the time-averaged current is 2π. From Fig. 6(a), we can also note that the average current is not polarized when only Rashba SOC is considered (black curve). This result is the same as shown in Fig. 3(a). As the magnetic flux φ increases, the spin up current and spin down current gradually separate. When $\varphi = \pi/2$, the polarization is as large as 100% for the given set of system parameters ($\sigma_R = \pi/2$ or $\sigma_R = 3\pi/2$). In the situation where $\varphi = \pi/2$, the transmitted electrons in the spin up channel can undergo constructive interference in the double QD system. However, at the same time, the spin down electrons undergo destructive interference, which results in the maximum of spin polarization. Therefore, a purely spin up current or spin down current can be chosen by adjusting the strength of the Rashba SOC for $\varphi = \pi/2$ case. In addition, there is no spin polarization when $\sigma_R = 2n\pi$. Thus, the spin polarized current can be regulated by the phase induced by Rashba SOC in an ac field. With increasing dc bias V, the magnitude of the spin polarization also increases significantly, as can be seen in Fig. 6(b).

B. Parallel double dots with a side-coupled dot ($t \neq 0$)

The effect of the coupling term t between the QD_2 and the QD_3 on the spin-dependent average current through the system described above is illustrated in Fig. 7. The spin-dependent average current in the case $t = \Gamma$ is quite different from the $t = 0$ case shown in Fig. 2(b). All the peaks of the spin up current, including the main peaks and sideband peaks, are split at $\varepsilon = n\hbar\omega$ and the split peaks of the spin down current disappear. From Eq. (11), we find that the split peaks are located at

$$\varepsilon = n\hbar\omega \pm \sqrt{t^2 - \Gamma^2 \sin^2\left(\frac{\varphi - s\sigma_R}{2}\right)}, \quad n = 0, \pm 1, \pm 2, \ldots. \tag{15}$$

These peaks all result from the PAT effect due to the coupling between QD_2 and QD_3, and each term in the sum in Eq. (11) can be viewed as the contribution from the coupling for n-photon processes. It should be noted that if $t = \Gamma$, the peaks for the spin down channel should appear at $\varepsilon = n\hbar\omega$, which is the position for conventional PAT peaks. It can be seen in Fig. 7(a) that the shape of the spin up peaks, $\varepsilon = n\hbar\omega \pm \sqrt{t^2 - \frac{1}{2}\Gamma^2}$, is distinctly different from that of the

spin down peaks, which correspond to another kind of sideband peak. Due to quantum interference between the two paths for transmitted electrons (input lead-QD_1-output lead) and (input lead-QD_2-output lead), the current spectrum shows peaks in Fig. 2. The effect of the coupling between QD_2 and QD_3 is to modify the above quantum interference between the QD_1 path and QD_2 path. When $t=\Gamma$, the influence of coupling term has only a very small role. The appearance of the resonance peaks at $\varepsilon = n\hbar\omega \pm \sqrt{t^2 - \frac{1}{2}\Gamma^2}$ is due to the path of transmitted electron being from the input lead, through QD_2-QD_3-QD_2 to the output lead. A new quantum state can be formed by QD_2 and QD_3. When the coupling strength, t, between QD_2 and QD_3 increases, the change in the average current can be seen with significant modification of the quantum interference through the triple QD system. Therefore, a resonance band forms when the strength of coupling t is similar to Γ. The three PAT peaks thus occur in the average current as the value of t increases. Three quantum states can be formed by the triple QD, and the three PAT peaks can be seen clearly in Fig. 7(b). In Fig. 7(b), when $t=3\Gamma$, the spin up peaks and spin down peaks appear at approximately $\varepsilon = n\hbar\omega \pm t$ and $\varepsilon = n\hbar\omega$. It may be seen that the three PAT peaks for both spin channels can be clearly distinguished only when $t^2 \gg \Gamma^2$. The PAT peaks due to the coupling between QD_2 and QD_3 decrease when t is similar to Γ. That is, the PAT peaks induced by the coupling between QD_2 and QD_3 become smaller as t decreases. The three PAT peaks cannot be distinguished in the $t<\Gamma$ case.

Fig. 8(a) shows a numerical calculation of the spin-dependent average current $\langle I\rangle$ versus ε under asymmetric ac bias. For the $t=0$ case, a shoulder occurs on the left side of the main peak, and a negative current shoulder appears on the right side of the main peak. The negative current shoulder and the positive current shoulder in the curve are due to the electron-photon pump effect. With increased coupling, such as $t=\Gamma$ (weak-coupling), changes in the spin up channel caused by the coupling are too small to discern. However, the shoulder for spin down electrons is higher than for the $t=0$ case. The height of the shoulder is determined by the coupling. However, the location of the PAT shoulder is independent of the MW field amplitude and the coupling strength.

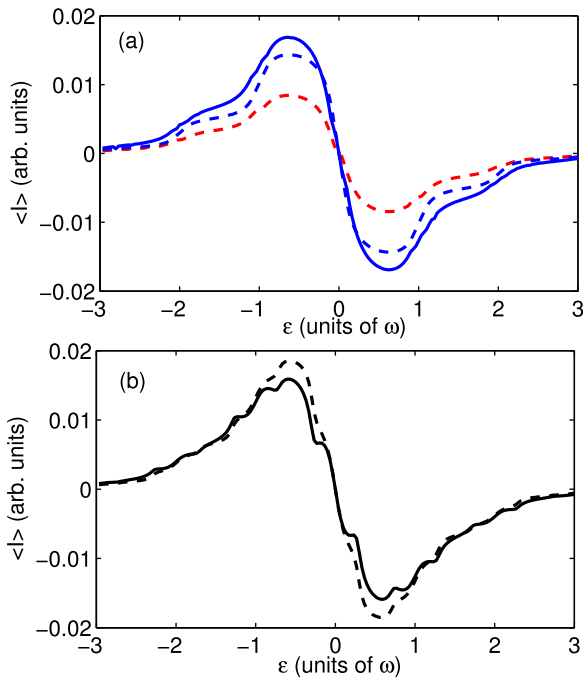

FIG. 8. Spin-dependent average currents, $\langle I\rangle_\uparrow$ (solid line) and $\langle I\rangle_\downarrow$ (dashed line), versus electron energy ε for two QDs connected in parallel with a side-coupled QD, under an asymmetric ac bias ($eW_L=0$, $eW_R=\hbar\omega=1$) with (a) $t=0$ (red line), $t=\Gamma=0.1$ (blue line), and (b) $t=3\Gamma=0.3$ (black line). The other parameters are $k_BT=0.001$, $V=0$, $\sigma_R=\pi/4$, $\varphi=\pi/4$, and $U=0$.

To examine the effects of strong coupling, we set $t=3\Gamma$, and use $W_L=0$, $W_R\neq 0$, with the source-drain voltage $V=\mu_L-\mu_R=0$. In this case, the transmitted electrons flowing in the left lead will be free of the MW fields, and only the transmitted electrons in the right lead feel the MW fields. The electron-photon pump effect appears as steps in the $\langle I\rangle$ versus ε curves as shown in Fig. 8(b). The locations of the shoulders due to the electron-photon pump are not only at $n\hbar\omega$ but also at $n\hbar\omega \pm t$. This means that the tunneling electron can emit or absorb photons with different frequencies in a more complicated way. For example, the electron for the $\varepsilon=0$ energy level can absorb or emit a photon of energy $n\hbar\omega$ in the usual manner. However, an electron in the $\varepsilon=\pm t$ energy level may also absorb or emit a photon of energy $n\hbar\omega$ with the result that coherence effects arise. The result is a more complicated multiple-PAT effect which is caused by two effects. The first effect is that the MW field and the coupling considered in the system cause the new quantum state corresponding to the three QDs to participate in the transmission. The second effect is that the MW field applied on the right lead in an asymmetric way induces the electron-photon pump effect.

IV. SUMMARY AND CONCLUSIONS

In summary, we have studied the PAT effect and the electron-photon pump effect through two QDs connected in parallel with a side-coupled QD, the whole system being irradiated by a MW field. The spin-dependent average currents $\langle I\rangle_\uparrow$, $\langle I\rangle_\downarrow$, the spin occupation n_{is} and spin accumulation Δn_i, were obtained utilizing the Keldysh nonequilibrium Green's function method. When only the Rashba SOC is considered, spin polarization can be produced in the QDs, and can be seen in the spin accumulation. When we consider the combined effect of both Rashba SOC and a magnetic flux, both the intradot occupation numbers and the time averaged current through the system are polarized. A pure spin polarized current can be generated due to the nonzero spin-dependent phase σ_R and the magnetic flux φ in the presence of an ac bias. This provides an efficient way to generate a pure spin polarization current in nanostructures. When QD_2 and QD_3 are coupled, several interesting effects related to the more complicated level structure of the QDs are expected to occur. In particular, the multiple-PAT effect is more complicated and a new kind of PAT peak obtained by controlling the strength of the coupling arises. The model considered here can be realized using present technologies. These results are expected to be useful for device design and quantum computation in the future.

ACKNOWLEDGMENTS

This work was supported by the National Natural Science Foundation of China (Grant Nos. 61176089 and 11104059), the Natural Science Foundation of Hebei Province (Grant Nos. A2011205092 and A2011208010). We are also very grateful to Professor N. E. Davison for the enhancement of the English writing.

[1]P. K. Tien and J. P. Gorden, Phys. Rev. **129**, 647 (1963).
[2]A. D. Stone, M. Y. Azbel, and P. A. Lee, Phys. Rev. B **31**, 1707 (1985).
[3]D. Sokolovski, Phys. Rev. B **37**, 4201 (1988).
[4]H. C. Liu, Phys. Rev. B **43**, 12538 (1991).
[5]P. Johansson, Phys. Rev. B **41**, 9892 (1990).
[6]P. Johansson and G. Wendin, Phys. Rev. B **46**, 1451 (1992).
[7]Y. V. Nazarov, Physica B **189**, 57 (1993).
[8]C. Bruder and H. Schoeller, Phys. Rev. Lett. **72**, 1076 (1994).
[9]X. B. Chen, D. P. Liu, W. H. Duan, and H. Guo, Phys. Rev. B **87**, 085427 (2013).
[10]N. S. Wingreen, A. P. Jauho, and Y. Meir, Phys. Rev. B **48**, 8487 (1993).
[11]A. P. Jauho, N. S. Wingreen, and Y. Meir, Phys. Rev. B **50**, 5528 (1994).
[12]L. Y. Chen and C. S. Ting, Phys. Rev. B **43**, 2097 (1991).
[13]E. Runge and H. Ehrenreich, Phys. Rev. B **45**, 9145 (1992).
[14]Q. F. Sun and T. H. Lin, J. Phys.: Condens. Matter **9**, 4875 (1997).
[15]K. Shibata, A. Umeno, K. M. Cha, and K. Hirakawa, Phys. Rev. Lett. **109**, 077401 (2012).
[16]R. N. Shang, H. O. Li, G. Cao, M. Xiao, T. Tu, H. W. Jiang, G. C. Guo, and G. P. Guo, Appl. Phys. Lett. **103**, 162109 (2013).
[17]K. Wang, C. Payette, Y. Dovzhenko, P. W. Deelman, and J. R. Petta, Phys. Rev. Lett. **111**, 046801 (2013).
[18]T. Obata, M. P. Ladrière, Y. Tokura, and S. Tarucha, New J. Phys. **14**, 123013 (2012).
[19]L. P. Kouwenhoven, S. Jauhar, K. McCormick, D. Dixon, P. L. McEuen, Yu. V. Nazarov, N. C. van der Vaart, and C. T. Foxon, Phys. Rev. B **50**, 2019 (1994).
[20]L. P. Kouwenhoven, S. Jauhar, J. Orenstein, P. L. McEuen, Y. Nagamune, J. Motohisa, and H. Sakaki, Phys. Rev. Lett. **73**, 3443 (1994).
[21]Q. F. Sun and T. H. Lin, Phys. Rev. B **56**, 3591 (1997).
[22]Q. F. Sun, J. Wang, and T. H. Lin, Phys. Rev. B **61**, 12643 (2000).
[23]X. T. An and J. J. Liu, Phys. Lett. A **372**, 6790 (2008).
[24]X. T. An, H. Y. Mu, Y. X. Li, and J. J. Liu, Phys. Lett. A **375**, 4078 (2011).
[25]X. T. An and J. J. Liu, Appl. Phys. Lett. **95**, 163501 (2009).
[26]Z. L. He and T. Q. Lü, Phys. Lett. A **376**, 2501 (2012).
[27]C. Guan, Y. H. Xing, C. Zhang, and Z. S. Ma, Appl. Phys. Lett. **102**, 163116 (2013).
[28]Q. F. Sun, J. Wang, and H. Guo, Phys. Rev. B **71**, 165310 (2005).
[29]W. G. van der Wiel, S. De Franceschi, J. M. Elzerman, T. Fujisawa, S. Tarucha, P. Blake, and L. P. Kouwenhoven, Rev. Mod. Phys. **75**, 1 (2002).
[30]F. Mireles and G. Kirczenow, Phys. Rev. B **64**, 024426 (2001).